Research Article | Vol. 26, No. 6 | 19 Mar 2018 | OPTICS EXPRESS 6532
Optics EXPRESS

Dielectrophoresis-actuated in-plane optofluidic lens with tunability of focal length from negative to positive

QINGMING CHEN,[1,2] TENGHAO LI,[1,2] YUJIAO ZHU,[1,2] WEIXING YU,[3] AND XUMING ZHANG[1,2,*]

[1]*Department of Applied Physics, The Hong Kong Polytechnic University, Hong Kong, China*
[2]*The Hong Kong Polytechnic University Shenzhen Research Institute, Shenzhen, 518057, China*
[3]*Key Laboratory of Spectral Imaging Technology, Xi'an Institute of Optics and Precision Mechanics, Chinese Academy of Sciences, Xi'an, Shaanxi, 710119, China*
**apzhang@polyu.edu.hk*

Abstract: This paper reports a tunable in-plane optofluidic lens by continuously tuning a silicone oil-air interface from concave to convex using the dielectrophoresis (DEP) force. Two parallel glasses are bonded firmly on two sides by NOA 81(Norland Optical Adhesive 81) spacers, forming an open microfluidic channel. An ITO (indium tin oxide) strip and another unpatterned ITO layer are deposited on two glasses as the top and bottom electrodes. Initially, a capillary concave liquid-air interface is formed at the end of the open channel. Then the DEP force is enabled to continuously deform the interface (lens) from concave to convex. In the experiment, the focal length gradually decreases from about −1 mm to infinite and then from infinite to around + 1 mm when the driving voltage is increased from 0 V to 260 V. Particularly, the longitudinal spherical aberration (LSA) is effectively suppressed to have LSA < 0.04 when the lens is operated in the focusing state. This work is the first study of in-plane tunable lenses using the DEP force and possesses special merits as compared to the other reported tunable lenses that are formed by pumping different liquids or by temperature gradient, such as wide tunability, no need for continuous supply of liquids, low power consumption (~81 nJ per switching) due to the capacitor-type driving, and the use of only one type of liquid. Besides, its low aberration makes it favorable for light manipulation in microfluidic networks.

OCIS codes: (130.3120) Integrated optics devices; (130.3990) Micro-optical devices; (220.3620) Lens system design.

References and links

1. D. Psaltis, S. R. Quake, and C. Yang, "Developing optofluidic technology through the fusion of microfluidics and optics," Nature **442**(7101), 381–386 (2006).
2. X. Fan and I. M. White, "Optofluidic Microsystems for Chemical and Biological Analysis," Nat. Photonics **5**(10), 591–597 (2011).
3. C. Monat, P. Domachuk, and B. J. Eggleton, "Integrated optofluidics: A new river of light," Nat. Photonics **1**(2), 106–114 (2007).
4. Z. Li, Z. Zhang, T. Emery, A. Scherer, and D. Psaltis, "Single mode optofluidic distributed feedback dye laser," Opt. Express **14**(2), 696–701 (2006).
5. S. I. Shopova, H. Zhou, X. Fan, and P. Zhang, "Optofluidic ring resonator based dye laser," Appl. Phys. Lett. **90**(22), 221101 (2007).
6. H. Schmidt and A. R. Hawkins, "Optofluidic waveguides: I. Concepts and implementations," Microfluid. Nanofluidics **4**(1-2), 3–16 (2008).
7. Y. Yang, A. Q. Liu, L. K. Chin, X. M. Zhang, D. P. Tsai, C. L. Lin, C. Lu, G. P. Wang, and N. I. Zheludev, "Optofluidic waveguide as a transformation optics device for lightwave bending and manipulation," Nat. Commun. **3**(1), 651 (2012).
8. L. K. Chin, A. Q. Liu, Y. C. Soh, C. S. Lim, and C. L. Lin, "A reconfigurable optofluidic Michelson interferometer using tunable droplet grating," Lab Chip **10**(8), 1072–1078 (2010).
9. J. Q. Yu, Y. Yang, A. Q. Liu, L. K. Chin, and X. M. Zhang, "Microfluidic droplet grating for reconfigurable optical diffraction," Opt. Lett. **35**(11), 1890–1892 (2010).

#318454 https://doi.org/10.1364/OE.26.006532
Journal © 2018 Received 26 Dec 2017; revised 13 Feb 2018; accepted 23 Feb 2018; published 5 Mar 2018

Optics EXPRESS

10. C. Song, N.-T. Nguyen, S.-H. Tan, and A. K. Asundi, "Modelling and optimization of micro optofluidic lenses," Lab Chip **9**(9), 1178–1184 (2009).
11. Y. C. Seow, S. P. Lim, and H. P. Lee, "Optofluidic variable-focus lenses for light manipulation," Lab Chip **12**(19), 3810–3815 (2012).
12. Y. Zhao, Z. S. Stratton, F. Guo, M. I. Lapsley, C. Y. Chan, S.-C. S. Lin, and T. J. Huang, "Optofluidic imaging: now and beyond," Lab Chip **13**(1), 17–24 (2013).
13. W. Song and D. Psaltis, "Pneumatically tunable optofluidic 2 × 2 switch for reconfigurable optical circuit," Lab Chip **11**(14), 2397–2402 (2011).
14. P. Müller, A. Kloss, P. Liebetraut, W. Mönch, and H. Zappe, "A fully integrated optofluidic attenuator," J. Micromech. Microeng. **21**(12), 125027 (2011).
15. S. Xiong, A. Q. Liu, L. K. Chin, and Y. Yang, "An optofluidic prism tuned by two laminar flows," Lab Chip **11**(11), 1864–1869 (2011).
16. B. S. Schmidt, A. H. Yang, D. Erickson, and M. Lipson, "Optofluidic trapping and transport on solid core waveguides within a microfluidic device," Opt. Express **15**(22), 14322–14334 (2007).
17. Y. Z. Shi, S. Xiong, L. K. Chin, Y. Yang, J. B. Zhang, W. Ser, J. H. Wu, T. N. Chen, Z. C. Yang, Y. L. Hao, B. Liedberg, P. H. Yap, Y. Zhang, and A. Q. Liu, "High-resolution and multi-range particle separation by microscopic vibration in an optofluidic chip," Lab Chip **17**(14), 2443–2450 (2017).
18. Y. Tung, M. Zhang, C. Lin, K. Kurabayashi, and S. J. Skerlos, "PDMS-based opto-fluidic micro flow cytometer with two-color multi-angle fluorescence detection capability using PIN photodiodes," Sens. Actuators B Chem. **98**(2), 356–367 (2004).
19. N. Wang, X. Zhang, Y. Wang, W. Yu, and H. L. W. Chan, "Microfluidic reactors for photocatalytic water purification," Lab Chip **14**(6), 1074–1082 (2014).
20. N. Wang, X. Zhang, B. Chen, W. Song, N. Y. Chan, and H. L. W. Chan, "Microfluidic photoelectrocatalytic reactors for water purification with an integrated visible-light source," Lab Chip **12**(20), 3983–3990 (2012).
21. K. Zhang, A. Jian, X. Zhang, Y. Wang, Z. Li, and H.-Y. Tam, "Laser-induced thermal bubbles for microfluidic applications," Lab Chip **11**(7), 1389–1395 (2011).
22. H. L. Liu, Y. Shi, L. Liang, L. Li, S. S. Guo, L. Yin, and Y. Yang, "A liquid thermal gradient refractive index lens and using it to trap single living cell in flowing environments," Lab Chip **17**(7), 1280–1286 (2017).
23. C. Song, T.-D. Luong, T. F. Kong, N.-T. Nguyen, and A. K. Asundi, "Disposable flow cytometer with high efficiency in particle counting and sizing using an optofluidic lens," Opt. Lett. **36**(5), 657–659 (2011).
24. N.-T. Nguyen, "Micro-optofluidic Lenses: A review," Biomicrofluidics **4**(3), 031501 (2010).
25. C. Fang, B. Dai, Q. Xu, R. Zhuo, Q. Wang, X. Wang, and D. Zhang, "Hydrodynamically reconfigurable optofluidic microlens with continuous shape tuning from biconvex to biconcave," Opt. Express **25**(2), 888–897 (2017).
26. X. Mao, S.-C. S. Lin, M. I. Lapsley, J. Shi, B. K. Juluri, and T. J. Huang, "Tunable Liquid Gradient Refractive Index (L-GRIN) lens with two degrees of freedom," Lab Chip **9**(14), 2050–2058 (2009).
27. H. T. Zhao, Y. Yang, L. K. Chin, H. F. Chen, W. M. Zhu, J. B. Zhang, P. H. Yap, B. Liedberg, K. Wang, G. Wang, W. Ser, and A. Q. Liu, "Optofluidic lens with low spherical and low field curvature aberrations," Lab Chip **16**(9), 1617–1624 (2016).
28. Q. Chen, A. Jian, Z. Li, and X. Zhang, "Optofluidic tunable lenses using laser-induced thermal gradient," Lab Chip **16**(1), 104–111 (2016).
29. C.-C. Cheng and J. A. Yeh, "Dielectrically actuated liquid lens," Opt. Express **15**(12), 7140–7145 (2007).
30. F. Krogmann, W. Mönch, and H. Zappe, "Electrowetting for tunable micro-optics," J. Microelectromech. Syst. **17**(6), 1501–1512 (2008).
31. F. Mugele and J.-C. Baret, "Electrowetting: from basics to applications," J. Phys. Condens. Matter **17**(28), R705–R774 (2005).
32. S. Xu, H. Ren, and S. T. Wu, "Dielectrophoretically tunable optofluidic devices," J. Phys. D Appl. Phys. **46**(48), 483001 (2013).
33. S. Kuiper and B. H. W. Hendriks, "Variable-focus liquid lens for miniature cameras," Appl. Phys. Lett. **85**(7), 1128–1130 (2004).
34. S.-K. Fan, H.-P. Lee, C.-C. Chien, Y.-W. Lu, Y. Chiu, and F.-Y. Lin, "Reconfigurable liquid-core/liquid-cladding optical waveguides with dielectrophoresis-driven virtual microchannels on an electromicrofluidic platform," Lab Chip **16**(5), 847–854 (2016).
35. H. Ren and S.-T. Wu, "Tunable-focus liquid microlens array using dielectrophoretic effect," Opt. Express **16**(4), 2646–2652 (2008).
36. H. Ren, H. Xianyu, S. Xu, and S.-T. Wu, "Adaptive dielectric liquid lens," Opt. Express **16**(19), 14954–14960 (2008).
37. S. Xu, Y.-J. Lin, and S.-T. Wu, "Dielectric liquid microlens with well-shaped electrode," Opt. Express **17**(13), 10499–10505 (2009).
38. H. Ren, S. Xu, D. Ren, and S.-T. Wu, "Novel optical switch with a reconfigurable dielectric liquid droplet," Opt. Express **19**(3), 1985–1990 (2011).
39. S.-K. Fan, T.-H. Hsieh, and D.-Y. Lin, "General digital microfluidic platform manipulating dielectric and conductive droplets by dielectrophoresis and electrowetting," Lab Chip **9**(9), 1236–1242 (2009).
40. T. B. Jones, "Liquid dielectrophoresis on the microscale," J. Electrost. **51**, 290–299 (2001).

Optics EXPRESS

41. Y. Zhu and K. Petkovic-Duran, "Capillary flow in microchannels," Microfluid. Nanofluidics **8**(2), 275–282 (2010).
42. L. Hu, M. Wu, W. Chen, H. Xie, and X. Fu, "Discontinuous pinning effect by a hole row to the gas-liquid interface in a parallel gap," Exp. Therm. Fluid Sci. **87**, 50–59 (2017).
43. K. Mishra, C. Murade, B. Carreel, I. Roghair, J. M. Oh, G. Manukyan, D. van den Ende, and F. Mugele, "Optofluidic lens with tunable focal length and asphericity," Sci. Rep. **4**(1), 6378 (2014).

1. Introduction

Optofluidics seamlessly integrates optics and microfluidics in a single chip to make full use of the advantages of both [1–3].It utilizes liquid as optical medium to replace conventional solid material, which enables unprecedented merits such as wide tunability of refractive index (RI), reconfigurability and easy integration with lab-on-a-chip systems. A variety of optical components have been demonstrated in optofluidics, such as light sources [4,5], optical waveguides [6,7], gratings [8,9], liquid lenses [10–12], optical switches [13], optical attenuators [14] and optofluidic prisms [15]. And the optofluidic systems have been used for numerous applications, including biosensors [2], particle manipulations [16,17], flow cytometry [18], photocatalysis [19,20], fluidic manipulation [21], etc. As a key component in optics, the optofluidic lens has attracted intensive interests from various communities. Among them, the in-plane liquid lenses, which provide a flexible way to manipulate and reshape the beam inside a chip, have found several applications in microfluidic networks [22,23]. Although the previous liquid lenses have demonstrated great compatibility and reconfigurability, new design of in-plane liquid lenses with better performance still attracts continuous research efforts for lab-on-a-chip applications.

The previous in-plane liquid lenses can be generally classified into two types: refractive lens and gradient index lens (GRIN lens) [24]. The former is often formed by laminar flow streams of immiscible liquids. The optically smooth fluidic interface can be utilized to focus the beam without significant scattering loss. The curvature of the interface can be modified by controlling the flow rate, thereby changing its focal length. Fang et al. demonstrated a hydrodynamically reconfigurable optofluidic lens using flowing streams, in which the liquid of high RI acts as the core and the other one of low RI as the cladding [25]. They demonstrated the tuning of the liquid lens from biconcave to biconvex by adjusting the flow rate. On the other hand, the GRIN lens is achieved by concentration diffusion or thermal gradient, in which a specific graded index profile can be obtained in microscale for light manipulation. Mao et al. proposed a Liquid Gradient Refractive Index (L-GRIN) for focusing light in a microfluidic chip [26]. They utilized the diffusion of $CaCl_2$ solution between side-by-side laminar flows to establish a hyperbolic scant (HS) RI profile. By precisely controlling the mixing between ethylene glycol and deionized water in an optofluidic chip, a low spherical and low field curvature aberrations lens was demonstrated by Ai Qun Liu's group [27].The thermal gradient can also be employed to form GRIN lenses. We presented a thermal lens for beam shaping based on laser-induced thermal gradient [28], which enables fast tuning and remote control. However, the above mentioned optofluidic lenses rely on the continuous flows, which require a lot of solution and external pumping. The complex structure and the continuous supply of liquids may limit the application of the optofluidic components.

Electrostatic force has also been widely used for adaptive liquid lenses [29,30]. According to the working principle, they can be classified into electrowetting lens [31] and dielectrophoresis (DEP) lens [32]. In the electrowetting lens, an external voltage is applied to modify the contact angle between the liquid and the lateral sidewall of the liquid container, thereby changing the droplet curvature as well as the focal length [33]. Real-time modulation of the focal length can be achieved by changing the applied voltage. And the DEP exerts a net force on the fluidic interface to drive the liquid of greater permittivity into the strong electric field region originally occupied by the medium of smaller permittivity [34]. Most of the previous electric liquid lenses are out-of-plane lens, like the conventional solid lens, the

Optics EXPRESS

beams are manipulated in the direction perpendicular to the microfluidic substrate [35–38]. They have been used to replace the conventional solid lenses in some specific circumstances. But the poor compatibility of the out-of-plane lenses limits their application in microfluidic networks.

This paper proposes a new type of in-plane optofluidic lens actuated by the DEP force (also named as liquid dielectrophoresis [39,40]). In an open microfluidic channel, a thin layer of silicone oil is sandwiched between two glasses, one has a patterned straight strip as the top electrode and the other has a uniform ITO layer as the bottom electrode. Initially, a concave liquid-air interface is formed at the end of the open microchannel by capillary flow [41]. Then, the electric field exerts a net DEP force to continuously modify the liquid-air interface as well as the focal length.

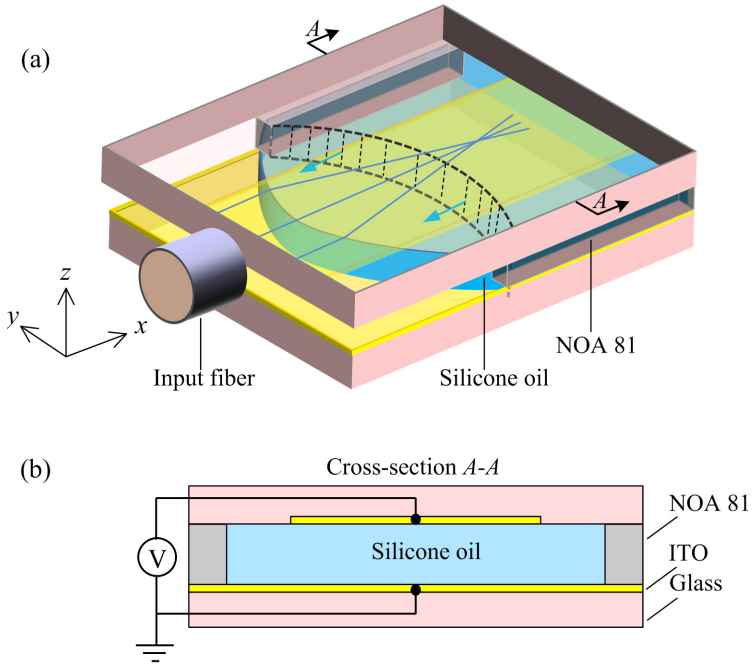

Fig. 1. Schematic design of the DEP lens. (a) 3D view, the DEP force drives the liquid-air interface from concave (dashed line: initial state) to convex. (b) Cross-sectional view of the lens, which has a top electrode (at the center of the channel) and a bottom electrode, the liquid layer is sandwiched by the two glasses bonded and spaced by two NOA 81 adhesive strips.

2. Working principle

The schematic design of the reconfigurable DEP liquid lens is shown in Fig. 1. Two MgF_2 glasses are used as the top and bottom, which are bonded firmly by two NOA 81 strips, forming an open channel (length 10 mm, width 0.6 mm, height 55 μm). Silicone oil (n = 1.405) is chosen as the optical medium, which can be easily filled into the open channel by the capillary force. The cross-section view in Fig. 1(b) shows that an ITO strip (width 400 μm, thickness 100 nm) is deposited on the top glass as the anode and an ITO thin layer (thickness 100 nm) on the bottom glass as the ground. In the initial state, a concave interface (indicated by the dashed line in Fig. 1(a)) is formed at the end of the channel, resulting in a divergent lens. When a DC voltage is applied to the device, an electric field is generated in between the two glasses. According to the liquid dielectrophoresis, the DEP force drives the silicone oil ($\varepsilon_{silicone}$ = 2.5) into the air region. As a result, the liquid-air interface is deformed into a convex shape (blue liquid in Fig. 1(a)). The curvature of the interface can be continuously tuned by changing the applied voltage. To visualize the lensing effect, a

Optics EXPRESS

collimated probe beam (waist diameter 400 μm) is coupled into the liquid layer from left to right (i.e., from air to liquid in Fig. 1(a)) using a pigtailed aspheric fiber collimator (CFS2-532-FC, beam divergence 1.75 mrad, Thorlabs).

The DEP force exerted at the liquid-air interface between two parallel plates can be expressed as [39,40]

$$F_e = \frac{\varepsilon_0 (\varepsilon_L - 1) w}{2d} V^2 \tag{1}$$

where $\varepsilon_0$is the permittivity of vacuum and ε_L is the relative permittivity of the liquid. And w is the width of the ITO strip and $d$is the gap between the two glasses. It is noted that the DEP force is dependent on the dielectric property of liquid and the applied voltage.

The pressure drop at the liquid-air interface can be described by the Laplace law [42]

$$\Delta \mathrm{P}_0 = 2\gamma\kappa = \gamma\left(\frac{1}{R_{10}} + \frac{1}{R_{20}}\right) \tag{2}$$

here γ is the surface tension between silicone oil and air, and κ is the mean curvature of the liquid-air interface. R_{10}(in horizontal) andR_{20} (in vertical) are the principal curvature radii of a point at the interface. The liquid-air interface is assumed to be spherical, which will be validated by the experiment later. Initially, the capillary force in the microchip is balanced. When an external voltage is applied, it changes the curvature as well as the pressure difference. As the surface property of the top and bottom surfaces is constant, R_{20}keeps unchanged [42]. The pressure variation is

$$\Delta \mathrm{P}_1 - \Delta \mathrm{P}_0 = \gamma\left(\frac{1}{R_{11}} + \frac{1}{R_{20}}\right) - \gamma\left(\frac{1}{R_{10}} + \frac{1}{R_{20}}\right) = \gamma\left(\frac{1}{R_{11}} - \frac{1}{R_{10}}\right) \tag{3}$$

It implies that the pressure variation only depends on the horizontal curvature radius. Because the extra pressure difference is induced by the DEP force, they should be equivalent [40]. Thus

$$F = (\Delta \mathrm{P}_1 - \Delta \mathrm{P}_0) w_0 d_0 = F_e \tag{4}$$

where w_0 and $d_0$are the width and height of the channel, respectively. Therefore, the curvature radius of the interface under new equilibrium can be calculated by Eqs. (1-4).In a spherical liquid-air interface, the focal length of the paraxial rays is described by

$$f = \frac{nR}{n-1} \tag{5}$$

here n *is* the refractive index of the liquid and R is the curvature radius of the interface. The light strikes on the interface from the air. In spherical lens, there is a longitudinal shift of focal length for the paraxial rays and the marginal rays. It is longitudinal spherical aberration (LSA) [43]. For example, in a convex lens, the marginal rays are focused closer to the lens, leading to a positive LSA value. In this paper, the edge pinning effect is used to suppress the LSA. More details will be presented below.

3. Experimental and simulated results

3.1Liquid-air interface measurement and ray tracing simulation

Experiments were conducted to demonstrate the DEP-actuated liquid lens. At first, a small amount of silicone oil was placed at the inlet of the open channel. Due to the capillary force, the liquid automatically flowed into the channel and stopped at the other end of the channel, resulting in a concave liquid-air interface (see Fig. 2(a1)). The initial liquid-air interface

Optics EXPRESS

matched closely aspherical curve (red dashed line) with a radius of −404 μm. Then a voltage was applied to the ITO electrodes, generating an electric field between the two plates. With the increase of voltage, the DEP force deformed the interface from initially concave to flat and then convex continuously. At 100 V, the magnitude of the interfacial radius became larger (see the dashed line in Fig. 2(a2), the calculated radius is −574 μm and the DEP force is $F_e = 4.83 \times 10^{-7}$ N,). A flat interface appeared at 180 V ($F_e = 1.57 \times 10^{-6}$ N), see Fig. 2(a3). Further increase of the voltage resulted in a convex shape. Figure 2(a4) exemplifies the interface under 260V ($F_e = 3.27 \times 10^{-6}$ N). It is noted that there is a deviation between the theoretical spherical curve (red dashed line) and the captured image (white dash-dot line) at the margin (see the enlarged view in Fig. 2(a5)). It is because of the edge pinning effect, which constrains the liquid-air interface at the lateral side, resulting in a smaller curvature at the margin of the interface. A ray tracing simulation was conducted to theoretically analyze the focusing performance of the convex lens (see Fig. 2(b)), showing that the parallel beams are well focused into a single point. This implies that the LSA is lower in the real liquid interface as compared to the ideal spherical interface. Detailed data will be presented below.

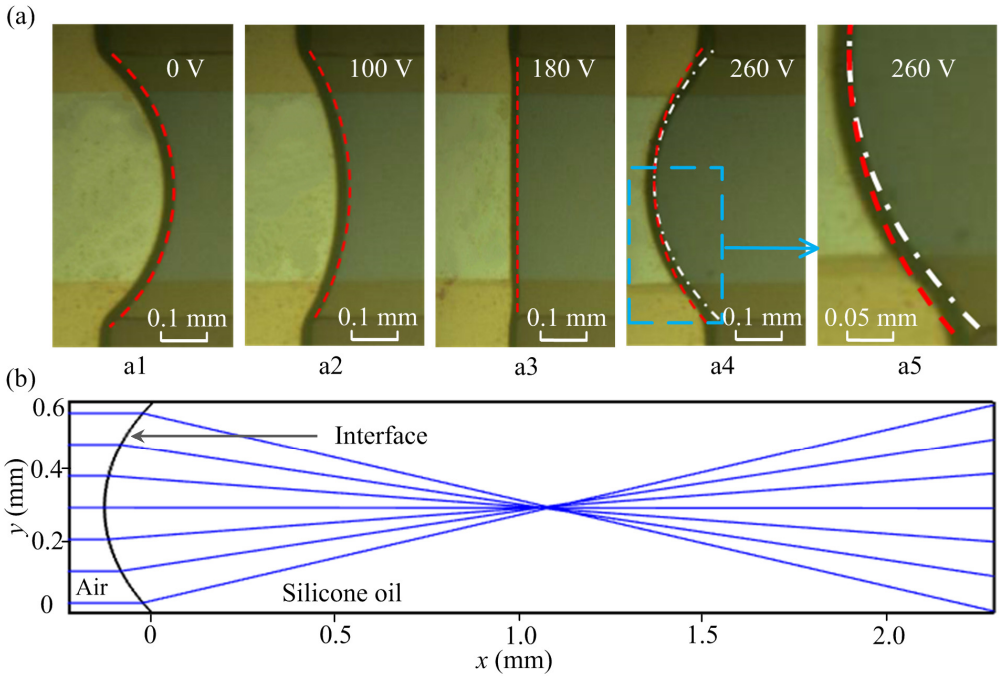

Fig. 2. Measurement and calculation of the liquid-air interface. (a) Experimental measurements of the interface under 0 V (i.e. initial state), 100 V, 180 V and260 V, respectively. The red dashed lines represent the ideal spherical interface. The white dashed-dotted line in a4 is the real interfacial curve derived from the captured image. And a5 is the enlarged view of the contact line of a4. (b) Ray tracing calculation of the measured liquid-air interface in a4.

3.2 Experimental analysis of the focusing performance

To experimentally trace the light path inside the microfluidic chip, the silicone oil was added with fluorescent dye Nile Red, which absorbs green light and emits fluorescence for easy visualization using the CCD imaging. Figure 3 presents the observed focusing states of the DEP-actuated liquid lens. A collimated probe beam (λ = 532 nm, waist diameter400 μm, optical power 10 mW) was coupled into the chip and propagated from air to silicone oil (i.e., from left to right in Fig. 3). Initially (i.e., at 0 V), the interface was concave by the balance of the surface tension, working effectively as a divergent lens (see Fig. 3(a)). Then an external voltage was applied to the two parallel plates, generating an electric field in the liquid layer.

Optics EXPRESS

The applied voltage was gradually increased from 0 V at a step of 5V. At 180 V, a flat interface appeared (see Fig. 3(b)). It has no focusing effect on the collimated probe beam. With further increase of the voltage, the DEP force deformed the liquid-air interface into a convex lens, converging the beam to a focal point (see Fig. 3(c)). By applying a voltage of 260 V, a minimum focal length of about 1 mm was obtained. Figure 3(d) shows that the beam is well converged into a focal point, matching the ray tracing simulation in Fig. 2(b).

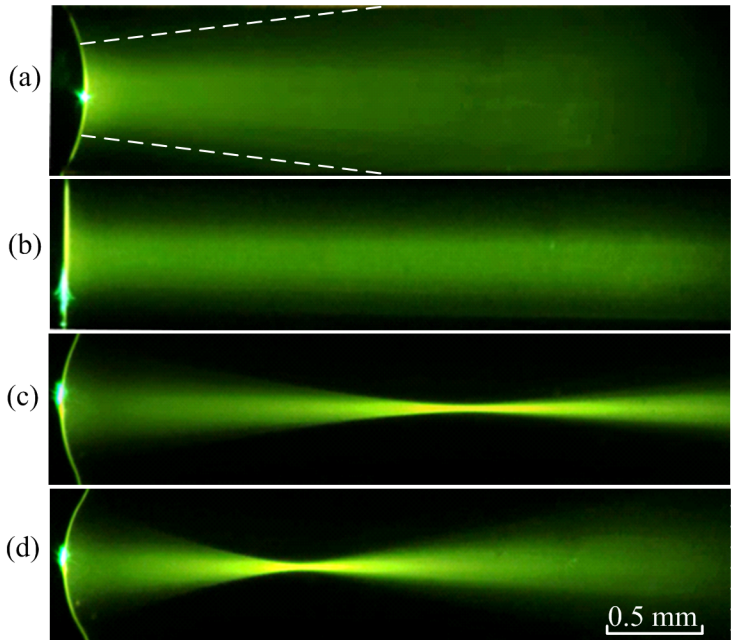

Fig. 3. Experimentally observed focusing states at different applied voltages. (a) Initial state: the parallel probe beam becomes divergent after passing through the liquid-air interface. (b) Flat interface at 180 V: the probe beam keeps parallel in the liquid medium. (c) Focusing state: the probe beam is converged with the further increase of the voltage. (d) A minimum focal length of about 1 mm is achieved at 260 V.

For quantitative analysis, the relationship between the focal length and the applied voltage is plotted in Fig. 4. To put the data of the divergent state (blue circles and blue line) and convergent state (black circles and black line) in one figure, they are plotted using different axes, as indicated by the arrows. When the voltage increases from 0 V to 180 V, the focal length declines from −1 mm to infinite (top and right axes). When the voltage is further increased, it turns into a convex lens. The focal length gradually decreases from infinite to about 1mm (at 260 V). In Fig. 4, the lines represent the calculated focal length (paraxial beam) and the data points are the experimental results. Each data point is an average of five independent measurements. The experimental result is in good agreement with the theoretical predication. Therefore, the spherical approximation provides a reliable way to predict the focus performance of the DEP-actuated optofluidic lens.

Due to the edge pinning effect, the contact line is partially pinned at the terminal of the open channel. This pinning effect reduces the marginal curvature (when it turns into convex), thereby suppressing the LSA. Figure 5 displays the comparison between the LSAs of the ideal spherical lens and the experimental lens. Here the LSA is represented by $\Delta f/f$, where f is the focal length of paraxial rays and Δf is the difference of focal lengths between the paraxial rays and the marginal rays. For the ideal spherical lens, the LSA is always positive and looks significant at short focal length (see black squares and black line in Fig. 5). With the increase of focal length, the LSA drops monotonically. In contrast, the experimental interface has a

Optics EXPRESS

negative LSA at short focal length and approaches the trend of the spherical lens for f> 2.8 mm. The color section in Fig. 5 indicates that the LSA of the experimental interface is limited to the range of −0.03 ~ + 0.04 (maximum magnitude 0.04), while that of the spherical interface is over + 0.01 ~ + 0.135 (maximum magnitude 0.135). The experimental interface has much smaller magnitude of LSA than the spherical interface. This implies that the suppressed LSA is an intrinsic merit of the DEP-actuated liquid lens. The two insets in Fig. 5 illustrate the LSAs of the spherical and experimental interfaces, respectively. In the spherical interface, the marginal rays are focused closer to the interface, this is the reason for the positive value of LSA. In the DEP-actuated convex liquid-air interface, the marginal rays cross each other just behind the paraxial focal point, leading to a smaller but negative value of LSA.

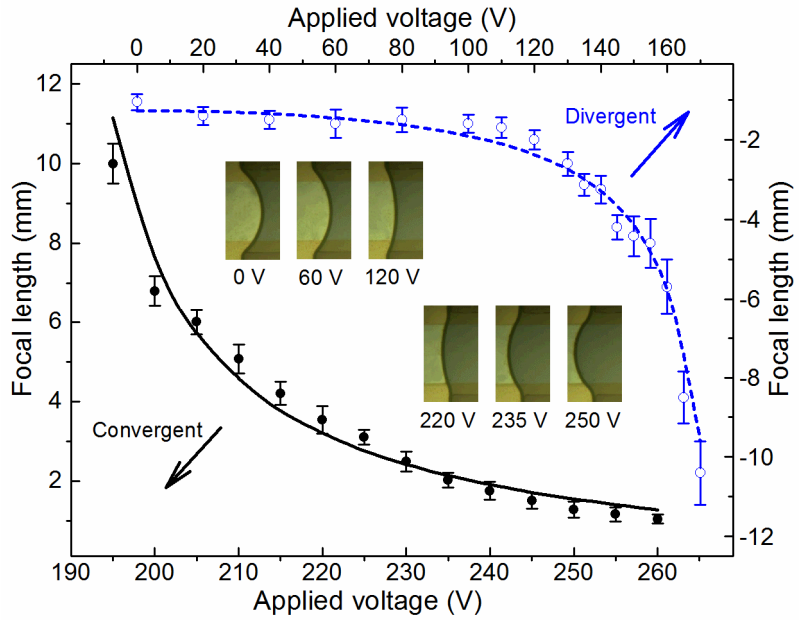

Fig. 4. The calculated (the curves) and the experimental (data points) focal lengths under different driving voltage. When the voltage is increased from 0 to 180 V, the focal length decreases from about −1 mm to infinite (top and right axes). While the voltage keeps increasing, the lens turns into a convex one and the focal length gradually decreases from infinite to about + 1 mm (the bottom and left axes). The insets show the observed liquid-air interfaces under 0 V, 60 V, 120 V, 220 V, 235 V and 250 V for easy visualization.

The power consumption can be estimated by treating the device as a parallel-plate capacitor. The measured resistance of the device is > 500 MΩ, showing its good insulation. The open channel has the dimensions 10 mm × 0.6 mm × 55 μm (L × W × H), and the silicone oil has the relative permittivity of 2.5, then the capacitance of the device is about 2.4 pF. In one charging process from 0 to 260 V, the consumed electrical energy is estimated to be 81 nJ per switching process, well showing the merit of low power consumption of this device.

We also investigated the hysteresis and the durability of the device. It is observed that the interface shapecan be well restored to its original state after the driving voltage is changed and then returned to the original value. Therefore, the device has very good repeatability and negligible hysteresis. It has also very good durability. Continuous operation for about one month has been demonstrated in the experiment, with little change of the focusing properties. This may be due to the low evaporation of the silicone oil in air.

Optics EXPRESS

The only problem is the slow response. The response time depends on the magnitude of the voltage variation. For instance, it takes about 4 s to switch from the initial concave state to the convex one with the shortest focal length and then stabilize in the final state. And the response is continuous, i.e., it goes continuously from the initial state to the new balanced state when the voltage experiences a step change. The width of the channel has significantly influence on the "response time". This is because there are two forces (i.e., the DEP force and the surface tension from the lateral sides) that play important roles in the lens system. A broad channel leads to a slow response. Another factor is the viscosity of the liquid, which describes the resistance to the deformation of liquid. The liquid with higher viscosity moves slower.

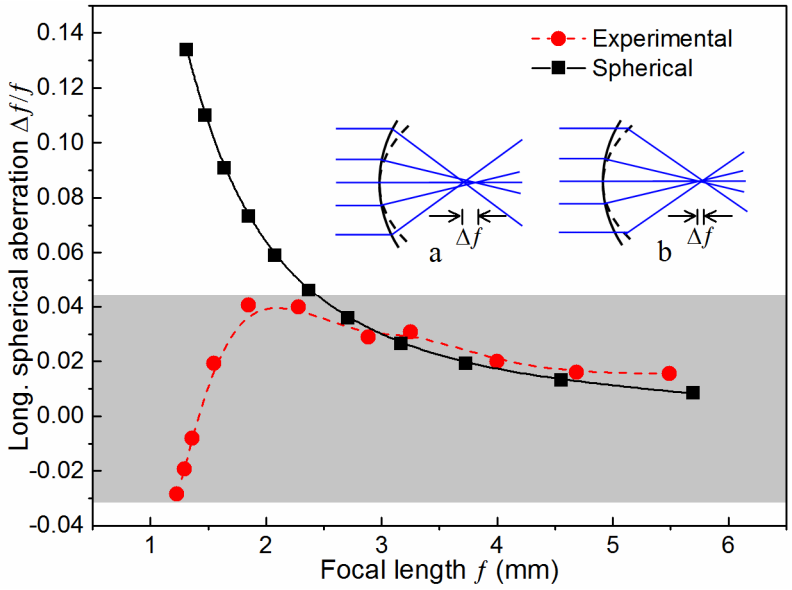

Fig. 5. Comparison of the longitudinal spherical aberrations $\Delta f/f$ of the experimental interface and the ideal spherical interface. The two insets show the ray tracing of the spherical (a) and the experimental interfaces (b), respectively. In the insets, the solid black line represents the spherical interface, and the black dashed line stands for the experimental interface.

4. Conclusion

In summary, a DEP-actuated reconfigurable optofluidic lens has been demonstrated for in-plane light manipulation. It utilizes the DEP force to continuously modify the fluidic lens from concave to convex. The proposed liquid lens has some intrinsic merits: low power consumption (~81 nJ per switching), easy fabrication, static liquid flow (low liquid consumption) and wide tunability of focal length from negative to positive. The low evaporation rate of the silicone oil makes the liquid lens stable and well repeatable. More importantly, the longitudinal spherical aberration of the convergent lens is effectively suppressed (the magnitude of measured LSA is below 0.04). There are also some limitations of the proposed lens. For example, it takes about 4s to switch from the initial concave state to the convex one with the shortest focal length; and it needs to be located at the end of the channel. Nevertheless, the simple design and the flexible tuning method make it suitable for microfluidic network integration and potential applications in lab-on-chip systems.

Funding

National Natural Science Foundation of China (no. 61377068 and 61361166004); Research Grants Council (RGC) of Hong Kong (the General Research Fund including N_PolyU505/13, PolyU 152184/15E and PolyU 152127/17E); The Hong Kong Polytechnic University (G-YBPR, 4-BCAL, 1-ZE14, 1-ZE27 and 1-ZVGH).

Optics EXPRESS

Acknowledgments

The technical assistance and facility support from Materials Research Centre, University Research Facility in Material Characterization and Device Fabrication, and University Research Facility in Life Sciences of the Hong Kong Polytechnic University.